# Total Hadronic ($\pi^-$, Ar) Cross Section for Run-II

Authors: Jonathan Asaadi, Elena Gramellini

**Abstract**

Puppa

# Contents

# 1 Tracking Studies

## 1.1 Angular Resolution

In this section, we outline the procedure used to evaluate the performance of the tracking algorithm in data and MC and the relative results. Scope of this study is to understand and compare the tracking performances and angular resolution of the TPC tracking on data and MC. We use the angular resolution of the tracking to determine the value of smallest angle that we can reconstruct with a non-zero efficiency, effectively determining a selection on the angular distribution of the cross section measurement due to the tracking performance.

We start by selecting all the WC2TPC matched tracks used for the cross section analysis. These tracks can contain from a minimum of 3 3D-space points to a maximum of 240 3D-space points. We fit a line to all the 3D space points associated with the track. For each track we calculate the average distance between each 3D point in space and the fit line as follows

$$\bar{d} = \frac{\sum_i^N d_i}{N}, \tag{1}$$

where $N$ is the number of point of the track and $d_i$ is the distance of the $i$-th space point to the line fit. Several tests to compare the goodness of fit between data and MC have been considered. We decided to use $\bar{d}$ for its straightforward interpretation. The $\bar{d}$ distribution for data and MC is shown in Figure 1 and shows a relatively good agreement between data and MC.

A visual representation of the procedure used to evaluate the angular resolution is shown in Figure 3. For each track, we order the space points according to their Z position along the positive beam direction (panel a) and we split them in two sets: the first set contains all the points belonging to the first half of the track and the second set contains all the points belonging the second half of the track. We remove the last four points in the first set and the first four points in the second set, so to have a gap in the middle of the original track (panel b). We fit the first and the second set of points with two lines (panel c). We then calculate the angle between the fit of the first and second half $\alpha$ (panel d). The angle $\alpha$ determines the spatial resolution of the tracking. The distributions for data and MC for $\alpha$ are given in Figure 2. The mean of the data and MC angular resolution are respectively

$$\bar{\alpha}_{Data} = (5.0 \pm 4.5) \text{ deg} \tag{2}$$

$$\bar{\alpha}_{MC} = (4.5 \pm 3.9) \text{ deg.} \tag{3}$$

Interaction angles smaller than the angle resolution are indistinguishable for the reconstruction. Therefore, we assess our ability to measure the cross section to be limited to interaction angles greater than 5.0 deg. More accurate studies of the angular resolution as a function of the kinetic energy and track length, albeit interesting, are left for an improvement of the analysis. A small 0.5 deg systematic shift between the mean of the data and MC angular resolution is present.

It is beneficial to take a moment to describe the definition of interaction angle. In case of elastic scattering, the definition is straightforward: the interaction angle is the angle between the incoming and outgoing pion, i.e.

$$\theta = \cos^{-1}\left( \frac{\vec{p}_{\text{incoming}} \cdot \vec{p}_{\text{outgoing}}}{|\vec{p}_{\text{incoming}}||\vec{p}_{\text{outgoing}}|} \right). \tag{4}$$

In case of inelastic scattering, the presence of several topologies requires a more complex definition, as shown in figure 4. We define the scattering angle as the biggest of the angles between the incoming pion and the visible daughters, where the visible daughters are charged particles that travel more than 0.47 cm in the detector (see panel a); in case all the daughters are invisible, the angle is assigned to be 90 deg (see panel b). We chose this working definition of scattering angle for inelastic scattering keeping in mind how our tracking reconstruction works: the tracking will stop correctly in case of all the daughters are not visible in the detector and it is likely to stop correctly if multiple daughters form an interaction vertex. The only "dangerous" case is the production of one charged daughter plus neutrals, which we can study with this working definition of scattering angle (see panel c).

We can see the effects of the angular resolution on the cross section by plotting the true Geant4 cross section for interaction angles greater than a minimum interaction angle. Figure 5 shows the true Geant4 cross section for interaction angles greater than 0 deg (green), 4.5 deg (red), 5.0 deg (blue) and 9.0 deg (yellow).
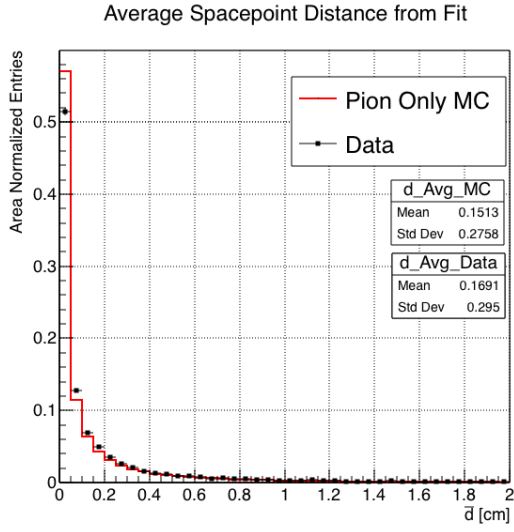
Figure 1: Distributions of the average distance between each 3D point in space and the fit line, $\bar{d}$ for the data used in the pion cross section analysis and the pion only DDMC. The distributions are area normalized.
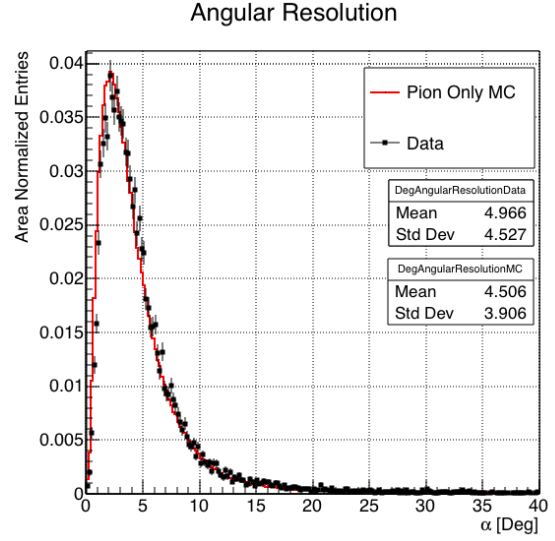


Figure 2: Distributions of angular resolution $\alpha$ for data used in the pion cross section analysis and pion only DDMC. The distributions are area normalized.
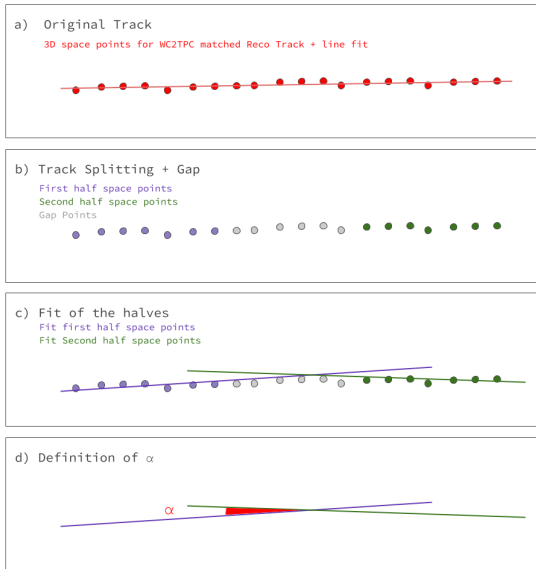


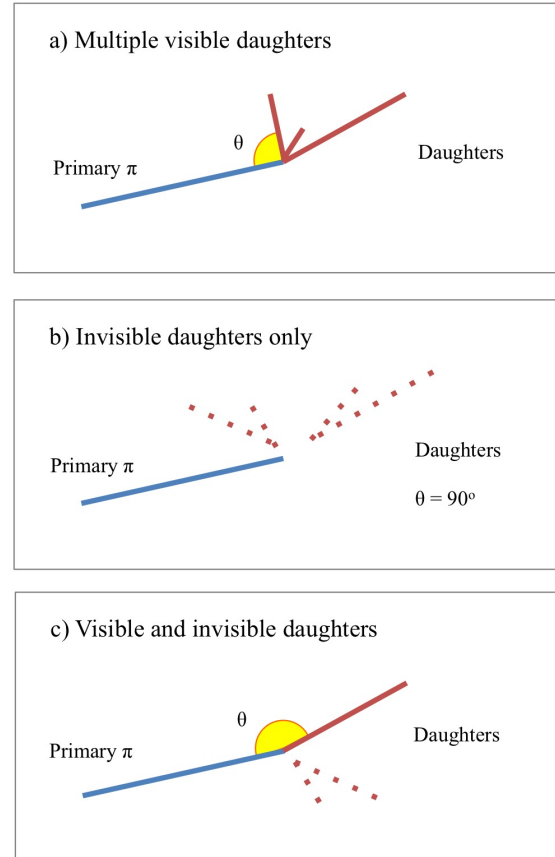Figure 3: A visual representation of the procedure used to evaluate the angular resolution.



Figure 4: A visual representation of the scattering angle definition in case of inelastic scattering.
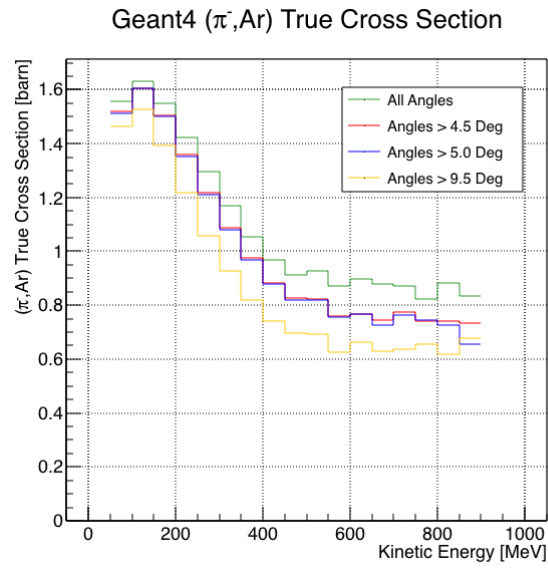
Figure 5: True $(\pi^--, Ar)$ cross section for interaction angles greater than 0 deg (green), 4.5 deg (red), 5.0 deg (blue) and 9.0 deg (yellow).

## 2  Energy Studies

A study we did was to look at the difference between DATA/MC in the dE/dX and energy deposited. We basically found there is very little difference between the two and we try to quantify how much the difference is.

### 2.1  dE/dX

Figure 6 shows the output of the fit of the Pion MC and the 60 Amp data. The MC is normalized to the data and both are fit to a Landau function. [a]
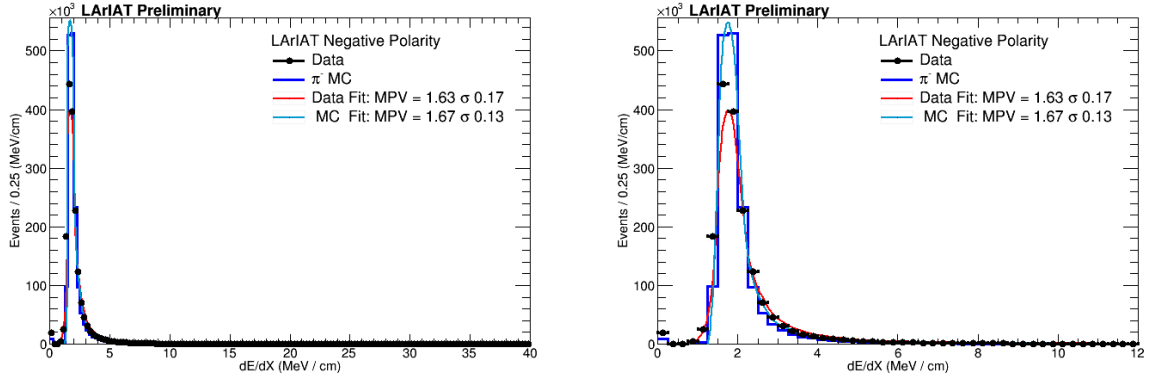


Figure 6: dE/dX for 60Amp data and data driven pion MC, both fit with a Landau

The difference between the two MPV's, is 2.4% between the data and the MC.

Figure 7 shows the stacked version of the dE/dX with the backgrounds stacked. The backgrounds are given in the ratio of 68.8% pion, 4.6% muon, and 26.6% electron. Once they are taken in these ratios, the sum of the MC is normalized to the sum of the data.
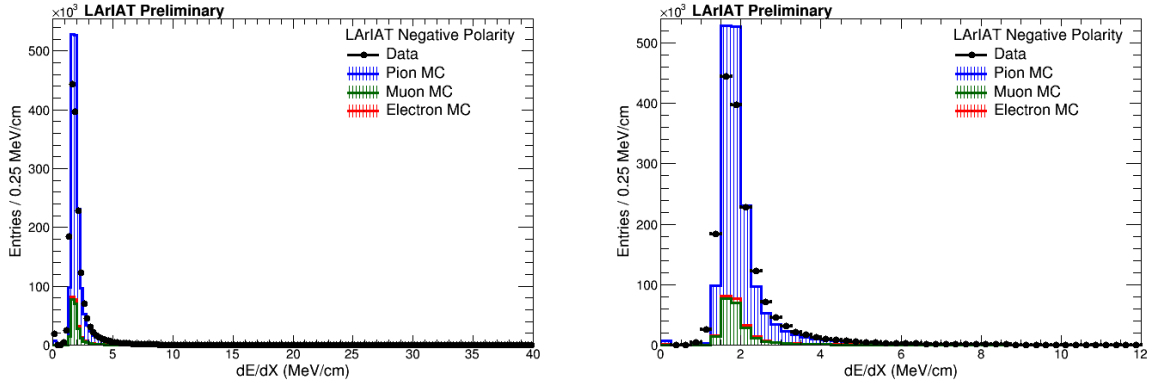


Figure 7: Stacked versions of the dE/dX with the data and electron/muon/pion MC.

For completeness, the log scale versions of are shown in Figure 8.
Plotting scripts can be found here on lariatgpvm

```
/lariat/app/users/jasaadi/v06_34_01_PionWeek/PlottingScripts
```

and the samples were put here

```
/lariat/data/users/elenag/theFinalPions/TPCDATA
```

```
/lariat/data/users/elenag/theFinalPions/TPC_MC/
```

---

[a]The entries at dE/dX = 0 come from an uninitialized variable and can/should be taken out of these plots
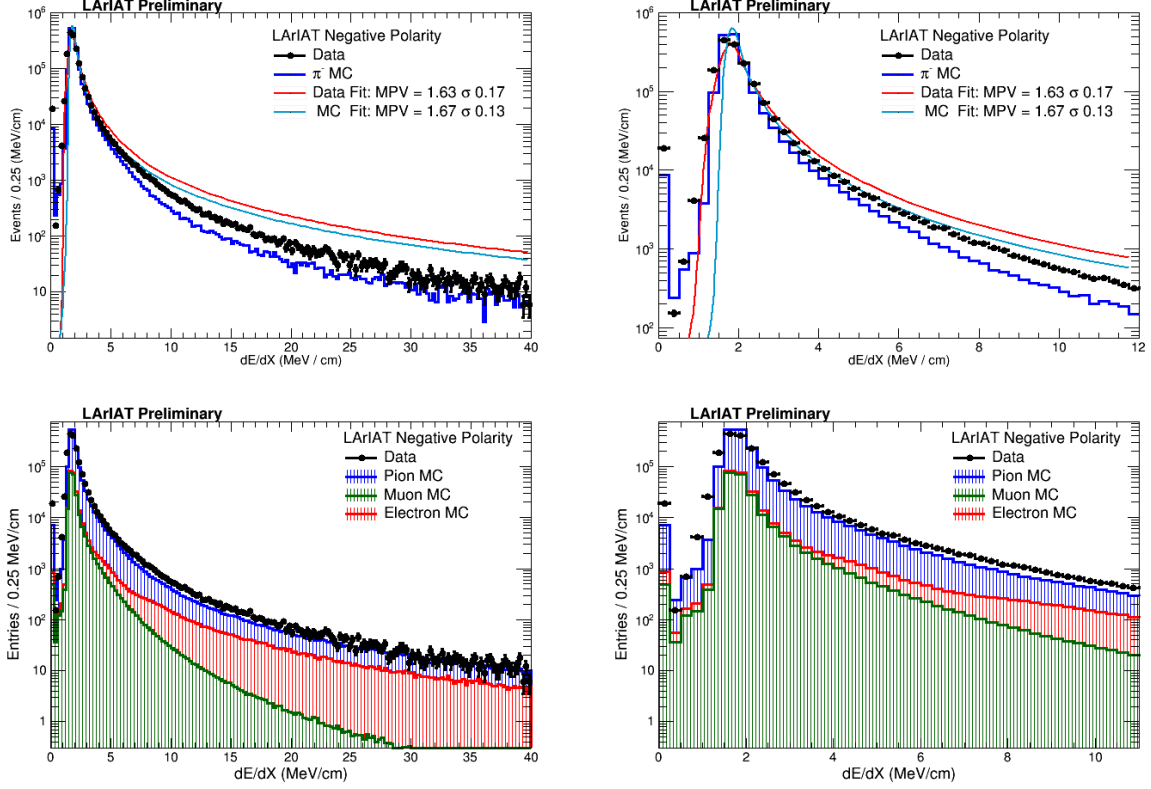
Figure 8: dE/dX for 60Amp data and MC shown in log scale

## 2.2 Energy Deposited

The initial energy the particle has as it enters the TPC is given by

$$KE_{Initial} = \sqrt{P_{WCtrk}^2 + m_\pi^2} - m_\pi^2 - E_{Loss} \tag{5}$$

and the uncertainty of the initial energy $\delta KE_{Initial}$ is given by

$$\delta KE_{Initial} = \sqrt{\delta P_{WCtrk}^2 + \delta E_{Loss}^2} \tag{6}$$

If we assume the uncertainty is 2% as the Minerva experiment had, and our uncertainty on the energy loss upstream is 7 MeV, then the total uncertainty on the initial kinetic energy for a typical 500 MeV pion is $\sim$ 12 MeV.

Now the energy for $j^{th}$ slab of the incident histogram is given by

$$KE_j^{Incident} = KE_{Inital} - (\sum_{i<j} dE/dX_i \times Pitch_i) \tag{7}$$

where $i$ is given by the slab you are at, $dE/dX_i$ is the energy deposited at that slab, and $Pitch_i$ is the pitch for that point.

Thus we can talk about the energy at the $j^{th}$ slab as

$$E_j^{slab} = (\sum_{i<j} dE/dX_i \times Pitch_i) \tag{8}$$

The systematic uncertainty of $E_j^{slab}$ is given by the difference between this quantity in data and MC, and the uncertainty on $E_j^{slab}$ is given by the width of the Landau fit to the data. These are shown in Figure 9

The difference between the MPV of data and MC is 1.0% (0.0784 - 0.0776 / 0.0784) and thus the systematic uncertainty you would assign to the energy in the incident kinetic energy would be for all 240 slices (assuming you have 240 slices at 0.4 mm pitch) and thus is

$$\delta E_j^{Slab} = (0.0784 - 0.0776) \times 240 = 0.008 MeV \times 240 = 1.92 MeV \tag{9}$$
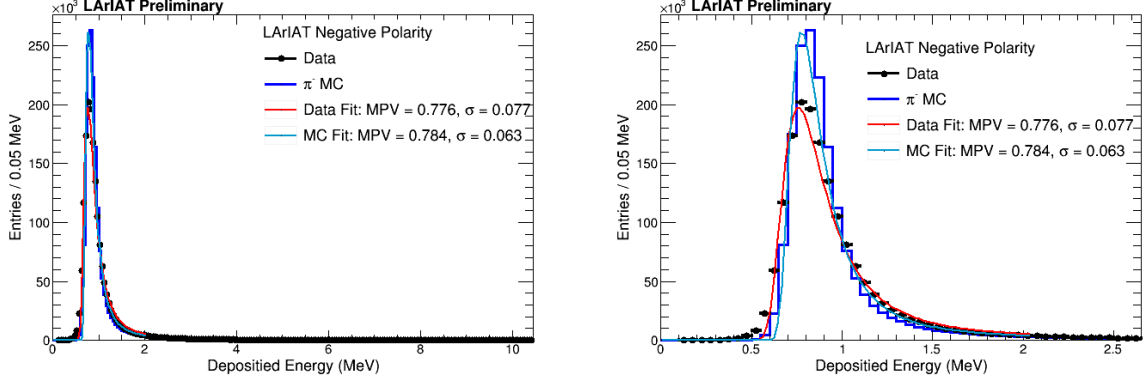
Figure 9: Energy Deposited in Pion MC and 60A data.

So the uncertainty on the incident kinetic energy is given by

$$\delta KE^{Incident} = \sqrt{(\delta KE_{Initial})^2 + (\delta E_j^{Slab})^2} = \sqrt{(12 MeV)^2 + (2 MeV)^2} = 12.1 MeV \qquad (10)$$

Figure 10 shows the stacked version of the Energy Deposited plots with the backgrounds stacked. The backgrounds are given in the ratio of 68.8% pion, 4.6% muon, and 26.6% electron. Once they are taken in these ratios, the sum of the MC is normalized to the sum of the data.



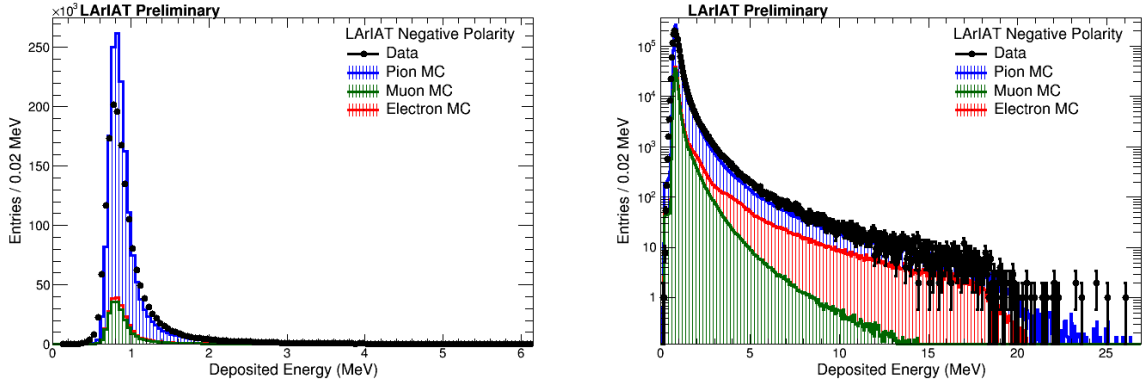Figure 10: Energy Deposited with all the MC and 60A data.

The energy at the interacting point is given by

$$KE_{Interaction} = \sqrt{P_{WCtrk}^2 + m_\pi^2} - E_{Loss} - (\Sigma dE/dX_i \times Pitch) \qquad (11)$$

and has the exact same uncertainty as the incident kinetic energy plot. Thus these estimates can be applied to getting the uncertainty on the energy of the reconstructed cross-section.

# 3  Outline Of the Measurement

If LArIAT had a beam of pure pions and were 100% efficient in determining the interaction point within the TPC, the pion cross section in each energy bin would be given by

$$\sigma^{\pi^-}(E_i) = \frac{1}{n\delta X} \frac{N_{Interacting}^{\pi^-}(E_i)}{N_{Incident}^{\pi^-}(E_i)}. \tag{12}$$

Unfortunately, this is not the case. The selection used to isolate pions in the LArIAT beam allows for the presence of some muons and electrons as background. Also, the LArIAT TPC is not 100% efficient in determining the interaction point. Therefore we need to apply two corrections in order to extract the true pion cross section from LArIAT data: the background subtraction and the efficiency correction. We estimate the true pion cross section in each energy bin changing the equation 12 into

$$\sigma^{\pi^-}(E_i) = \frac{1}{n\delta X} \frac{N_{Interacting}^{\pi^-}(E_i)}{N_{Incident}^{\pi^-}(E_i)} = \frac{1}{n\delta X} \frac{\epsilon_i^{inc}[N_{Interacting}^{TOT}(E_i) - B_{interacting}(E_i)]}{\epsilon_i^{int}[N_{Incident}^{TOT}(E_i) - B_{incident}(E_i)]}, \tag{13}$$

where $N_{Interacting}^{TOT}(E_i)$ and $N_{Incident}^{TOT}(E_i)$ is the measured content of the data interacting and incident histograms respectively, $B_{interacting}(E_i)$ and $B_{incident}(E_i)$ represent the contributions from beamline background, and $\epsilon_i^{int}$ and $\epsilon_i^{inc}$ are the efficiency corrections for said histograms.

As we will show in section 4.2, the background subtraction for the interacting and incident histograms can be translated into a corresponding corrections $C_{Interacting}^{\pi MC}(E_i)$ and $C_{Incident}^{\pi MC}(E_i)$ and the cross section re-written as follows

$$\sigma^{\pi^-}(E_i) = \frac{1}{n\delta X} \frac{\epsilon_i^{inc} N_{Interacting}^{TOT}(E_i) C_{Interacting}^{\pi MC}(E_i)}{\epsilon_i^{int} N_{Incident}^{TOT}(E_i) C_{Incident}^{\pi MC}(E_i)}. \tag{14}$$

The following sections describe the procedures used to evaluate the background subtraction (section 4) and the efficiency correction (section 5.1), as well as their uncertainties. The reader might be concerned about bin-by-bin migration of events in the interacting and incident plots due to the finite resolution of the energy reconstruction. In section 2.2, we make an argument to why we expect the smearing matrix to be extremely close to diagonal, such that its calculation and relative corrections are left for an improvement of the analysis.

# 4  Background Subtraction

Even if pions are by far the biggest component of the beam in negative polarity runs, the LArIAT beam is not a pure pion beam. While useful to discriminate pions/muons/electrons from kaons, and protons, the beamline detectors are not sensitive enough to discriminate among the lighter particles in the beam: electrons, muons and pions fall under the same mass hypothesis. Thus, we need to assess the background from beamline particles other than pions in the event selections used for the pion cross section analysis and correct for its effects.

## 4.1  Beam Composition

We define beamline background every TPC track matched to the WC track which is not a primary pion. Potentially, there are 4 different types of beamline background:

    1) electrons,

    2) muons,

    3) secondaries from pion events,

    4) matched pile up events.

The first step is to estimate what percentage of events used in the cross section calculation is not a primary pion. The next two sections will illustrate this estimate for the electrons, muons and secondaries from pion event. We estimate the last type of background, the "matched pile up" events, to be a negligible fraction, because of the definition of the WC2TPC match: we deem the probability of a single match with a halo particle in the absence of a beamline particle[b] negligibly small. SHOW VTX distribution in WC2TPC match

---

[b] Events with multiple WC2TPC matches are always rejected.

### 4.1.1 Background from Beamline Electrons and Muons

We estimate the percentage of electrons and muons in the beam via the G4Beamline MC. Since the beamline composition is a function of the magnet settings, we simulate separately events for magnet current of -60A and -100A. Table 1 shows the beam composition per magnet setting after the mass selection according to the G4Beamline simulation.

Figure 11 shows the momentum predictions from G4Beamline overlaid with data for the 60A runs (left) and for the 100A runs (right). The predictions for electrons, muons and pions have been staggered and their sum is area normalized to data, which is shown in red. Albeit not perfect, these plots show a reasonable agreement between the momentum shapes in data and MC. We attribute the difference in shape to the lack of simulation of the WC efficiency in the MC which is momentum dependent and leads to enhance the number events in the center of the momentum distribution.

Once the beam composition at WC4 is know, we simulate the electrons, muons and pions with the DDMC and we subject the three samples to the same selection chain (WC2TPC match, shower filter, pile up filter). The percentage of electrons and muons surviving the selection chain weighted by the beam composition is the electron and muon background in the pion cross section sample, as shown in Table 2.

### 4.1.2 Background from secondaries at TPC Front Face

Pions can travel the length of the LArIAT beamline and interact hadronically in the steel or in the non-instrumented argon upstream to the TPC front face. Or, they could decay in flight between WC4 and the TPC. One of the interaction products can leak into the TPC and be matched with the WC track, contributing to the pool of events used for the cross section calculation. We call this type of particles "secondaries" from pion events, with a terminology inspired by Geant4. We estimate the number of secondaries using the DDMC pion sample. The percentage of secondaries is given by the number of matched WC2TPC tracks whose corresponding particle is not flagged as primary by Geant4. The secondary to pion ratio is 4.9% in the 60A sample and $Y\%$ in the 100A sample.

## 4.2 Background Contribution to the Cross Section

Once we have estimated the beam composition, the next step is propagating pions, muons and electrons to the TPC and evaluate their collective contribution to the cross section. To do so, we simulate the same number of electrons, muons and pions with the DDMC and we apply the same selection filters on the three samples. The number of events per particle species surviving this selection is shown on table 2.

In order to reproduce the closest make up of the beam to data, we weight each event of a given particle species according to the estimated beam composition. In case of 60A runs, for example, the weights are
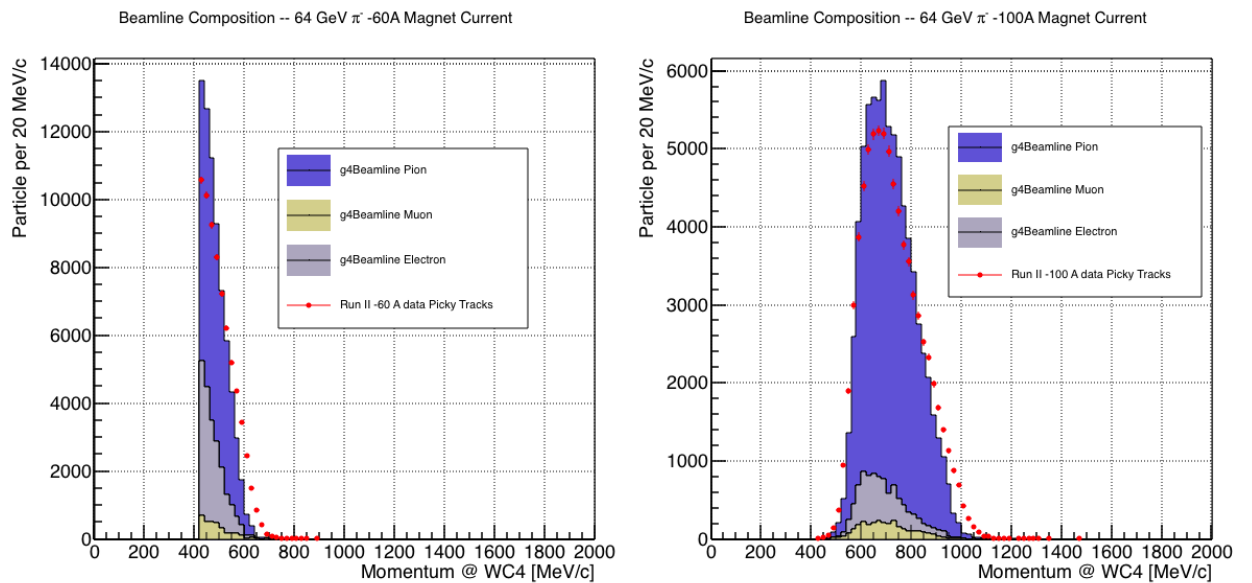


Figure 11: Beam composition for the -60A runs (left) and -100A runs (right). The solid blue plot represents the simulated pion content, the yellow plot represents the simulated muon content and the grey plot represents the simulated electron content. The plots are area normalized to the number of data events, shown in red.

|            | I = -60 A | I = -100 A |
|------------|-----------|------------|
| G4Pions    | 68.8 %    | 87.4 %     |
| G4Muons    | 4.6 %     | 3.7 %      |
| G4Electrons| 26.6 %    | 8.9 %      |

Table 1: Simulated beamline composition per magnet settings

|                            | Magnet Current -60A | | | Magnet Current -100 A | | |
|                            | MC $\pi^-$ | MC $\mu^-$ | MC $e^-$ | MC $\pi^-$ | MC $\mu^-$ | MC $e^-$ |
|----------------------------|------------|------------|----------|------------|------------|----------|
| Total Initial events       | 334500     | 334500     | 334500   |            |            |          |
| After Multiplicity Rejection | 330668   | 333420     | 198065   |            |            |          |
| After WC2TPC Selection     | 218239     | 296333     | 91139    |            |            |          |
| Evts After Shower Rejection| 208063     | 288914     | 20293    |            |            |          |
| Selection Survival Rate    | 62.3%      | 86.6%      | 6.1%     |            |            |          |
| Beam Composition @WC4       | 68.8%      | 4.6 %      | 26.6 %   | 87.4 %     | 3.7 %      | 8.9 %    |
| Beam Composition @TPC FF    | 88.5%      | 8.2%       | 3.3 %    |            |            |          |

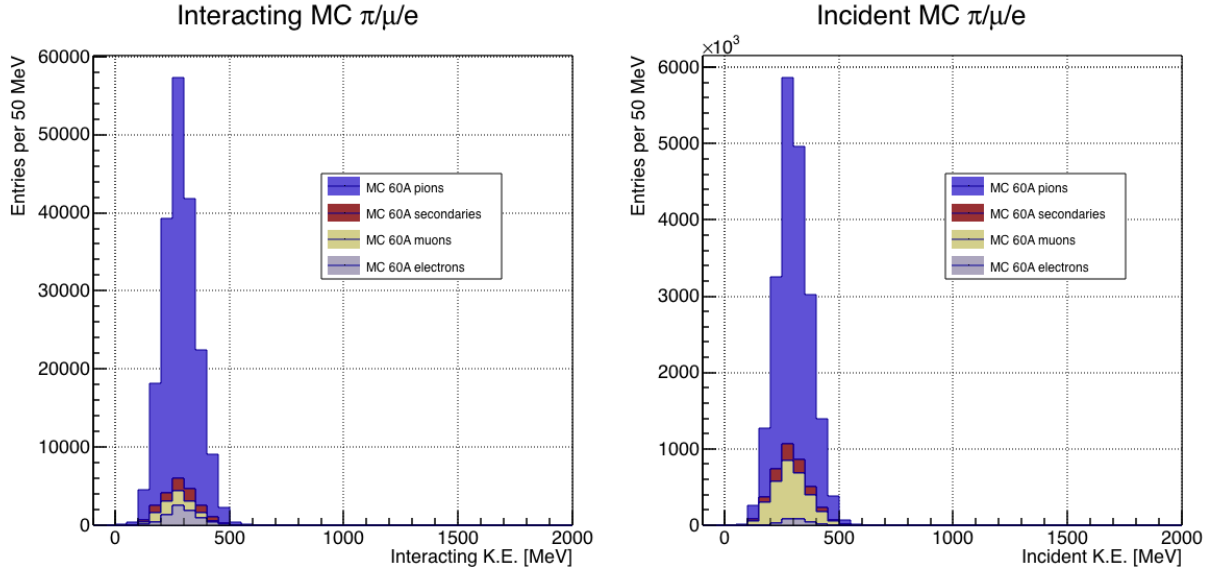Table 2: MC selection flow per particle species.



Figure 12: Left: staggered contributions to the interacting kinetic energy distribution for electron (grey), muons (yellow) and pion (blue) in the 60A simulation sample. Right: staggered contributions to the incident kinetic energy distribution for electron (grey), muons (yellow) and pion (blue) in the 60A simulation sample.

0.688 for pions, 0.046 for muons and 0.266 for electrons. We produce accordingly the interacting and incident histograms for the events surviving the selection, staggering the contributions for each particle species, as shown in Figure 12. From those histograms, we are able to evaluate the relative contribution of pions and background to each bin of the interacting and incident histograms separately and obtain the respective corrections for data. We take here the interacting histogram as example, noting that the derivation of the correction for the incident histogram is identical. The number of entries in each bin of the interacting plot (Figure 12 left) is $N^{TOT}_{Interacting}(E_i)$, equal to the sum of the pions and background in that bin, namely

$$N^{TOT}_{Interacting}(E_i) = N^{\pi}_{Interacting}(E_i) + \underbrace{N^{\mu}_{Interacting}(E_i) + N^{e}_{Interacting}(E_i) + N^{Secondary}_{Interacting}(E_i)}_{B_{Interacting}(E_i)}. \qquad (15)$$

Thus, the relative contribution of pions to each bin in MC can be calculated as follows

$$C^{\pi MC}_{Interacting}(E_i) = \frac{N^{\pi MC}_{Interacting}}{N^{TOTMC}_{Interacting}(E_i)} = \frac{N^{TOTMC}_{Interacting}(E_i) - B^{MC}_{Interacting}(E_i)}{N^{TOTMC}_{Interacting}(E_i)}. \qquad (16)$$

In order to evaluate the pion content of each bin in data, we scale the measured bin content by the corresponding pion contribution found in MC, as follows

$$N^{\pi RecoData}_{Interacting} = N^{TOTData}_{Interacting}(E_i) - B^{Data}_{Interacting}(E_i) = C^{\pi MC}_{Interacting}(E_i)N^{TOTData}_{Interacting}(E_i). \qquad (17)$$

Figures 13 show $C^{\pi MC}_{Interacting}(E_i)$ and $C^{\pi MC}_{Incident}(E_i)$ as a function of the kinetic energy for the 60A runs and their systematic uncertainty. We take a 100% systematic uncertainty on the muon and electron content: we calculate the extreme values of $C^{\pi MC}_{Interacting}(E_i)$ and $C^{\pi MC}_{Incident}(E_i)$ in each bin changing the beam composition for the configurations listed in Table 3.

| | Magnet Current -60A | | | Magnet Current -100 A | | |
|---|---|---|---|---|---|---|
| | MC $\pi^-$ | MC $\mu^-$ | MC $e^-$ | MC $\pi^-$ | MC $\mu^-$ | MC $e^-$ |
| Composition 2x muons | 64.2 % | 9.2 % | 26.6 % | 83.7 % | 7.4 % | 8.9 % |
| Composition 0.5x muons | 71.1 % | 2.3 % | 26.6 % | 89.2 % | 1.9 % | 8.9 % |
| Composition 2x Electrons | 42.2 % | 4.6 % | 53.2 % | 78.5 % | 3.7 % | 17.8 % |
| Composition 0.5x Electrons | 82.1 % | 4.6 % | 13.3 % | 91.9 % | 3.7 % | 4.4 % |

Table 3: Beam composition variation for the study of systematics due to beam contamination.
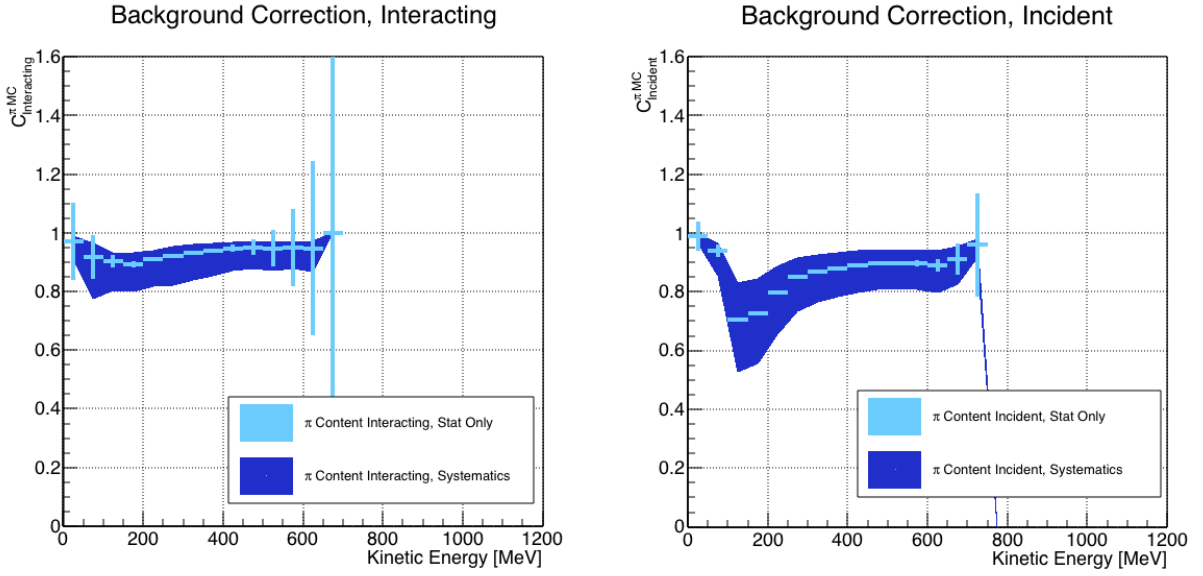


Figure 13: Left: relative pion content for interacting histogram a function of kinetic energy for the 60A runs, statistics uncertainty in azure and systematic uncertainty in blue. Right: relative pion content for incident histogram a function of kinetic energy for the 60A runs, statistics uncertainty in azure and systematic uncertainty in blue.

# 5    Efficiency Correction

The interaction point for a track used in the total hadronic cross section analysis is defined to be the last point of the WC2TPC matched track which lies inside the fiducial volume. This definition is independent from the topology of the interaction. If the TPC track stops within the fiducial volume, its last point will be the interaction point, no matter what the products of the interaction look like; if the track crosses the boundaries of the fiducial volume, the track will be considered "through going" and no interaction point will be found. Given this definition, it is evident that we rely on the tracking algorithm to discern where the interaction occurred in the TPC and correctly stop the tracking. The tracking algorithm has an intrinsic angle resolution as shown in section 1.1, which limits its efficiency, especially in the case of elastic scattering occurring a low angles. Thus, we need to apply an efficiency correction to data in order to retrieve the true cross section. The efficiency correction is evaluated separately for the interacting and incident histograms, namely $\epsilon_i^{int}$ and $\epsilon_i^{inc}$, and propagated to the cross section as shown in equation 13.

## 5.1    Efficiency Correction: Procedure

We describe here the procedure to calculate the efficiency correction taking the interacting histogram as example and noting that the procedure is identical for the incident histogram.

We derive the correction on a set of pure pion MC, calculating its value bin by bin as the ratio between the true bin content and the correspondent reconstructed bin content. The correction is then applied to the relevant bin in data. In formulae, the efficiency correction is calculated to be

$$\epsilon_i^{\text{int}} = \frac{N_{\text{Interacting}}^{\pi \text{ Reco MC}}(E_i)}{N_{\text{Interacting}}^{\pi \text{ True MC}}(E_i)}, \tag{18}$$

where $N_{\text{Interacting}}^{\pi \text{ True MC}}(E_i)$ is the content of the $i$-th bin in for the true interacting histogram, and $N_{\text{Interacting}}^{\pi \text{ Reco MC}}(E_i)$ is the content of the $i$-th bin in for the reconstructed interacting histogram. The correction is applied to data as follows

$$N_{\text{Interacting}}^{\pi \text{ True Data}}(E_i) = \frac{N_{\text{Interacting}}^{\pi \text{ Reco Data}}(E_i)}{\epsilon_i^{\text{int}}} = N_{\text{Interacting}}^{\pi \text{ Reco Data}}(E_i) \frac{N_{\text{Interacting}}^{\pi \text{ True MC}}(E_i)}{N_{\text{Interacting}}^{\pi \text{ Reco MC}}(E_i)}. \tag{19}$$

where $N_{\text{Interacting}}^{\pi \text{ Reco Data}}(E_i)$ is the background subtracted bin content of the $i$-th bin in for the reconstructed interacting histogram for data, i.e.

$$N_{\text{Interacting}}^{\pi \text{ Reco Data}}(E_i) = N_{\text{Interacting}}^{\text{TOT Data}}(E_i) - B_{\text{Interacting}}^{\text{Data}}(E_i) = C_{\text{Interacting}}^{\pi \text{ MC}}(E_i) N_{\text{Interacting}}^{\text{TOT Data}}(E_i). \tag{20}$$

Figures **??** show $\epsilon_i^{\text{int}}(E_i)$ and $\epsilon_i^{\text{int}}(E_i)$ as a function of the kinetic energy for the 60A runs and their systematic uncertainty.

In section 1.1, we estimated the angular resolution for data and MC to be $\bar{\alpha}_{Data} = (5.0 \pm 4.5)$ deg and $\bar{\alpha}_{MC} = (4.5 \pm 3.9)$ deg, respectively. Interaction angles smaller than the angular resolution are indistinguishable for the reconstruction. Thus, we claim we are able to measure the cross section for interaction angles greater than 5.0 deg. Geant4 simulates interactions at all angles, as shown in figure **??**. In order to calculate the efficiency correction, we select events which have an interaction angle greater than a given $\alpha_r es$ to construct the true interacting and incident histograms (the denominator of the efficiency correction).

The systematics on the efficiency correction is estimated by varying the value of $\alpha_r es$ to be
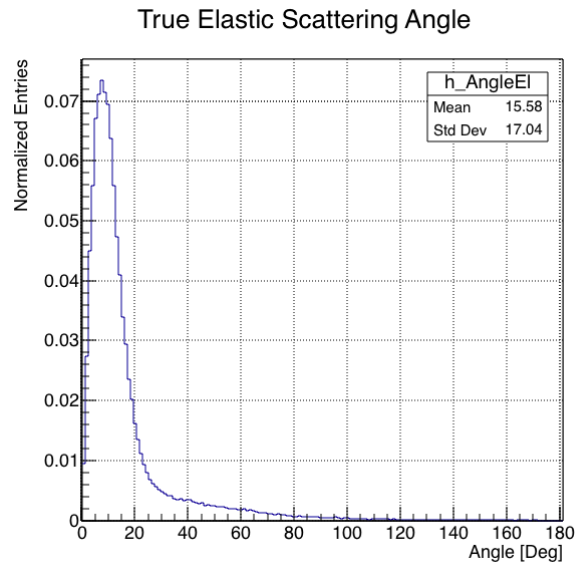
Figure 14: Distribution of the true scattering angle for a pion elastic scattering off the argon nucleus as simulated by Geant4.